Fine structure of exciton excited levels in a quantum dot with a magnetic ion

M. M. Glazov and E. L. Ivchenko
A.F. Ioffe Physico-Technical Institute, Russian Academy of Sciences, 194021 St.-Petersburg, Russia

L. Besombes, Y. Léger, L. Maingault, and H. Mariette
CEA-CNRS Group "Nanophysique et Semiconducteurs", Laboratoire de Spectrométrie Physique, CNRS and Université Joseph Fourier-Grenoble 1, BP 87, F-38402 St Martin d'Hères, France
(Received 25 November 2006; revised manuscript received 13 February 2007; published 10 May 2007)

The fine structure of excited excitonic states in a quantum dot with an embedded magnetic ion is studied theoretically and experimentally. The developed theory takes into account the Coulomb interaction between charged carriers, the anisotropic long-range electron-hole exchange interaction in the zero-dimensional exciton, and the exchange interaction of the electron and the hole with the *d* electrons of a Mn ion inserted inside the dot. Depending on the relation between the quantum dot anisotropy and the exciton-Mn coupling, the photoluminescence excitation spectrum has a qualitatively different behavior. It provides a deep insight into the spin structure of the excited excitonic states.

DOI: 10.1103/PhysRevB.75.205313 PACS number(s): 78.67.Hc, 75.75.+a, 78.55.Et

I. INTRODUCTION

Optical microspectroscopy is a set of powerful optical techniques that do not damage the sample and allow one to extract local quantitative information on micron and submicron scales. These high spatial resolution optical techniques have been used to measure the photoluminescence (PL) from single quantum dots and study the exchange interaction between a zero-dimensional exciton and a few[1,2] or a single magnetic ion embedded in the quantum dots (QDs).[3–7] Theoretically, the ground-state energy spectrum of a quantum dot containing a Mn ion was studied in Refs. 8–10.

In this work, we have theoretically and experimentally studied the fine structure of *excited* excitonic states in such magnetically doped QDs. We have developed a theory taking into account both direct Coulomb and long-range exchange interactions between an electron and a hole in the zero-dimensional exciton and exchange interaction of the coupled electron-hole pair with the Mn *d* electrons. The fine structure of the excited state is shown to be determined by an interplay of the anisotropic electron-hole long-range exchange interaction, the Coulomb interaction between the charge carriers, and the coupling of an exciton with a Mn ion.

The developed theory is compared with the PL excitation (PLE) measurements on an individual QD carrying a Mn^{2+} ion. The coupling constants of exciton-Mn interaction for the ground and optically active excited states are determined. The analysis of the fine structure of the excited states allows us to determine the degree of QD anisotropy and make conclusions about the magnetic ion position in a quantum dot.

The paper is organized in the following way. Section II is devoted to the theoretical analysis of the fine structure of *pp*-shell excitonic states in the QD without a Mn ion, Sec. III presents the results on the exciton interaction with the magnetic ion, and Sec. IV presents the experimental results and their analysis.

II. EXCITON STATES IN NONMAGNETIC DOTS

We consider heavy-hole exciton states in a single-quantum-well quantum dot. This means that we neglect heavy-hole–light-hole mixing and assume an exciton to be formed by a conduction-band electron with the spin $s=\pm 1/2$ and a heavy hole with the spin (or angular-momentum component) $j=\pm 3/2$.[6] For the in-plane confinement of free carriers, we choose *coaxial parabolic* potentials with z as the principal axis.[11] In what follows, we concentrate on QDs of sizes small enough to have the in-plane localization lengths for electrons (a_e) or holes (a_h) smaller than the two-dimensional (2D) exciton Bohr radius a_B.

To begin with, let us consider an axially (cylindrically) symmetric QD where the exciton ground state (*ss* shell) is described by the envelope

$$S(\rho_e,\rho_h)=\frac{1}{\pi a_e a_h}\exp\left(-\frac{\rho_e^2}{2a_e^2}-\frac{\rho_h^2}{2a_h^2}\right), \tag{1}$$

where $\boldsymbol{\rho}_{e,h}$ is the electron or hole in-plane radius vector with the components x_e, y_e or x_h, y_h referring to the center of the confining potential. Similarly, the *pp*-orbital excited states being the products of electron and hole $P_{x,y}$ orbitals have the forms

$$D_{xx}(\boldsymbol{\rho}_e,\boldsymbol{\rho}_h)=2\frac{x_e x_h}{a_e a_h}S(\rho_e,\rho_h),\quad D_{yy}(\boldsymbol{\rho}_e,\boldsymbol{\rho}_h)=2\frac{y_e y_h}{a_e a_h}S(\rho_e,\rho_h),$$

$$D_{xy}(\boldsymbol{\rho}_e,\boldsymbol{\rho}_h)=2\frac{x_e y_h}{a_e a_h}S(\rho_e,\rho_h),\quad D_{yx}(\boldsymbol{\rho}_e,\boldsymbol{\rho}_h)=2\frac{y_e x_h}{a_e a_h}S(\rho_e,\rho_h), \tag{2}$$

where the subscripts in D_{xx}, D_{yy}, D_{xy}, and D_{yx} describe the symmetry of the P orbitals for an electron and a hole.

In the isotropic parabolic potential, the four *pp*-shell states are degenerate. The Coulomb interaction between an electron and a hole lifts this degeneracy, see Fig. 1(a). The lowest-lying state with the wave function

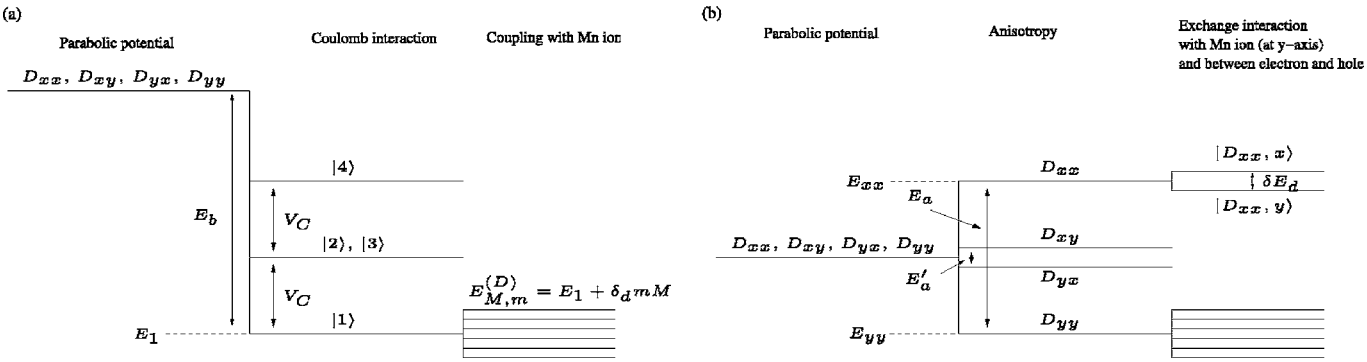

FIG. 1. Schematic *pp*-shell energy-level diagram for the (a) axial and (b) anisotropic QD. The energy splittings are shown not to scale.

$$|1\rangle = \frac{1}{\sqrt{2}}[D_{xx}(\boldsymbol{\rho}_e,\boldsymbol{\rho}_h) + D_{yy}(\boldsymbol{\rho}_e,\boldsymbol{\rho}_h)] \tag{3}$$

is optically active. The states $|2\rangle=[D_{xx}(\boldsymbol{\rho}_e,\boldsymbol{\rho}_h) - D_{yy}(\boldsymbol{\rho}_e,\boldsymbol{\rho}_h)]/\sqrt{2}$ and $|3\rangle=[D_{xy}(\boldsymbol{\rho}_e,\boldsymbol{\rho}_h)+D_{yx}(\boldsymbol{\rho}_e,\boldsymbol{\rho}_h)]/\sqrt{2}$ are degenerate and they are shifted above the state $|1\rangle$ by the energy

$$V_C = \frac{3\sqrt{\pi}}{4}\frac{\zeta^2}{(1+\zeta^2)^{5/2}}\frac{e^2}{\varkappa_0 a_e}, \tag{4}$$

where $\varkappa_0$ is the low-frequency dielectric constant and $\zeta = a_h/a_e$. The splitting between the pair of states $|2\rangle$, $|3\rangle$ and the highest state $|4\rangle=[D_{xy}(\boldsymbol{\rho}_e,\boldsymbol{\rho}_h)-D_{yx}(\boldsymbol{\rho}_e,\boldsymbol{\rho}_h)]/\sqrt{2}$ is given by V_C as well. The binding energy of the exciton $|1\rangle$ referring to the unperturbed position of *pp* orbitals reads

$$E_b = \frac{\sqrt{\pi}}{2}\frac{\zeta^4+5\zeta^2+1}{(1+\zeta^2)^{5/2}}\frac{e^2}{\varkappa_0 a_e}. \tag{5}$$

The parameters E_b and V_C completely determine the direct Coulomb interaction in the parabolic QD.

The energy separation between *ss* and *pp*-shell states is given by $\hbar(\Omega_e+\Omega_h)$, where

$$\Omega_e = \frac{\hbar}{m_e a_e^2}, \quad \Omega_h = \frac{\hbar}{m_h a_h^2}. \tag{6}$$

m_e and m_h are the electron and hole effective masses, respectively. If the parabolic potentials for electrons and holes are chosen in such a way that $\Omega_e=\Omega_h$, i.e., $m_e a_e^2 = m_h a_h^2$, these *pp*-shell states are exactly resonant with *sd* shells formed by the electron in the *s* shell and the hole in the *d* shell and vice versa.[11] For example, the $s_e d_h$-shell exciton envelope has the form

$$F(\boldsymbol{\rho}_e,\boldsymbol{\rho}_h) = \left(\frac{\rho_h^2}{a_h^2} - 1\right) S(\rho_e,\rho_h). \tag{7}$$

In this symmetric situation, *sd*-shell excitons are not optically active but they acquire the oscillator strength due to the Coulomb-induced mixing with *pp*-shell states. If the confinement is not symmetric, $m_e a_e^2 \neq m_h a_h^2$, the *sd*-shell states become optically active and are shifted from *pp* orbitals by the energy $\pm\hbar(\Omega_e-\Omega_h)$ (upper sign for $s_h d_e$ and lower sign for $s_e d_h$). However, the calculation shows that, as a rule, the oscillator strength for the *sd*-shell states is substantially smaller than that of the state $|1\rangle$ defined by Eq. (3). Moreover, for the best-fit parameters of a single QD studied experimentally in the present work (see below), the difference $\hbar(\Omega_e-\Omega_h)$ exceeds by far the matrix element of the Coulomb coupling between the *pp* and *sd*-shell states so that, in the first-order approximation, these states can be analyzed separately. Therefore, we focus on the fine structure of *pp*-shell states and, in the end of Sec. III, briefly discuss the exciton-Mn interaction for the *sd* state [Eq. (7)].

We next turn to the slightly elliptical QD where the effective localization radii a_e and a_h are replaced by localization lengths $a_{e,i}$ and $a_{h,i}$ $(i=x,y)$ in the x and y directions. The anisotropy is characterized by the ratios

$$\beta_e = \frac{a_{e,y}-a_{e,x}}{2a_e}, \quad \beta_h = \frac{a_{h,y}-a_{h,x}}{2a_h}.$$

For simplicity, we assume $\beta_e=\beta_h\equiv\beta$ and $\beta\ll 1$. The anisotropy fully lifts the degeneracy of *pp*-orbital states. In the case of large anisotropy (the criterion is given below), the splitting between two bright states $D_{xx}(\boldsymbol{\rho}_e,\boldsymbol{\rho}_h)$ and $D_{yy}(\boldsymbol{\rho}_e,\boldsymbol{\rho}_h)$ is given to the lowest order in β by

$$E_a = E_{xx} - E_{yy} = 4\beta\hbar(\Omega_e+\Omega_h), \tag{8}$$

where $\sigma=m_e/m_h$ characterizes the electron-hole mass ratio. The splitting between the dark states, $D_{xy}(\boldsymbol{\rho}_e,\boldsymbol{\rho}_h)$ and $D_{yx}(\boldsymbol{\rho}_e,\boldsymbol{\rho}_h)$, arises due to the difference between carrier masses and/or localization radii, namely,

$$E'_a = E_{xy} - E_{yx} = 4\beta\hbar(\Omega_e-\Omega_h). \tag{9}$$

The transition between the Coulomb-dominated and anisotropy-dominated regimes takes place at $|E_a| \sim V_C$.

The long-range exchange interaction affecting the bright exciton with $m=\pm 1$ is described by[12,13]

$$\mathcal{H}^{(\mathrm{long})}_{n'n} = \frac{1}{4\pi\varkappa_\infty}\left(\frac{e\hbar|p_0|}{m_0 E_g}\right)^2 \int d\boldsymbol{K}\frac{K^*_{m'}K_m}{K}\tilde{\psi}^*_{n'}(\boldsymbol{K})\tilde{\psi}_n(\boldsymbol{K}), \tag{10}$$

where n (or n') is the exciton-state index including both the angular-momentum component m (or m') and orbital state, $\varkappa_\infty$ is the high-frequency dielectric constant, $\boldsymbol{K}$ is the 2D center-of-mass wave vector with the components K_x, K_y,

$K_{\pm 1}=K_x \pm iK_y$, m_0 is the free electron mass, E_g is the band gap, p_0 is the interband matrix element of the momentum operator, and we introduced the 2D Fourier-transform $\tilde{\psi}(\boldsymbol{K}) = \int d\boldsymbol{\rho} e^{-i\boldsymbol{K}\boldsymbol{\rho}} \boldsymbol{\Psi}(\boldsymbol{\rho},\boldsymbol{\rho})$ of the exciton envelope function $\boldsymbol{\Psi}(\boldsymbol{\rho}_e,\boldsymbol{\rho}_h)$ taken at the coinciding coordinates, $\boldsymbol{\rho}_e=\boldsymbol{\rho}_h \equiv \boldsymbol{\rho}$. For the *ss* shell, $\boldsymbol{\Psi}_n(\boldsymbol{\rho},\boldsymbol{\rho})=S(\boldsymbol{\rho},\boldsymbol{\rho})$ and, for the *pp*-shell states $|D_{\alpha\beta},m\rangle$, $\boldsymbol{\Psi}_n(\boldsymbol{\rho},\boldsymbol{\rho})=D_{\alpha\beta}(\boldsymbol{\rho},\boldsymbol{\rho})$ with α and β running through x,y.

In the isotropic QD, the *ss*-shell radiative doublet is not split by the long-range interaction [Eq. (10)]. We introduce the characteristic value of the long-range exchange for *pp*-shell states,

$$\mathcal{E} = \left(\frac{e\hbar|p_0|}{m_0 E_g}\right)^2 \frac{\sqrt{\pi}}{16\varkappa_\infty a_e^3 \zeta \sqrt{1+\zeta^2}}. \tag{11}$$

For CdTe QD with $a_e=45$ Å, $a_h=90$ Å, $\varkappa_0=10.4$, $\varkappa_\infty=7.1$, $2p_0^2/m_0=17.9$ eV, and $E_g=1.6$ eV (see Ref. 12), the Coulomb-interaction-induced splitting $V_C \sim 3$ meV and $\mathcal{E} \sim 1.5\times 10^{-2}$ meV. Thus, $\mathcal{E} \ll V_C$ and the exchange interaction should be considered as a correction to the direct Coulomb interaction.[19] Therefore, in an axial QD, the exchange-induced splitting of the radiative *pp*-orbital doublet is proportional to $\mathcal{E}^2/V_C$ and can be neglected.

If the QD possesses an anisotropy in the axes x,y, the radiative doublet of the ground state [Eq. (1)] is split into a pair of linearly polarized sublevels with the microscopic dipole momentum parallel to x and y. This anisotropic splitting is given by

$$\delta E_s = 24\beta\mathcal{E} \tag{12}$$

and is proportional to the anisotropy degree β entering also into Eqs. (8) and (9). If anisotropic splitting E_a of the *pp* shells D_{xx}, D_{yy} exceeds the Coulomb energy V_C, each shell is additionally split into radiative sublevels $|D_{xx},x\rangle$, $|D_{xx},y\rangle$ or $|D_{yy},x\rangle$, $|D_{yy},y\rangle$ according to

$$\delta E_d = E_{|D_{xx},x\rangle} - E_{|D_{xx},y\rangle} = E_{|D_{yy},y\rangle} - E_{|D_{yy},x\rangle} = 3\mathcal{E}. \tag{13}$$

Comparing Eqs. (12) and (13), we conclude that splittings of the *ss* and *pp* shells differ by 8β.

III. INTERPLAY BETWEEN EXCITON-Mn AND ELECTRON-HOLE EXCHANGE INTERACTION

The Hamiltonian describing exciton-Mn exchange interaction can be conveniently represented in the basis of the certain components s, j, M of the electron, hole, and Mn-ion spins as

$$\mathcal{H}_{\mathrm{Mn}} = [A_e s\,\delta(\boldsymbol{r}_0-\boldsymbol{r}_e) + A_h j\,\delta(\boldsymbol{r}_0-\boldsymbol{r}_h)]M, \tag{14}$$

where $\boldsymbol{r}_0$ is the Mn-ion position, and A_e and A_h are the coupling parameters for conduction- and valence-band electrons.[14] In the derivation of Eq. (14), we took into account only $j=\pm 3/2$ hole states and neglected the interaction with the electron in-plane spin since, for the realistic set of parameters, $A_e < A_h/2$, see Refs. 3 and 10.

In a QD with an embedded Mn ion, the fine structure of the ground-state exciton is determined by the interplay between the QD anisotropy and the exchange coupling with the Mn ion. From now on, we consider the most important (from both experimental and theoretical points of view) case where the ground-state anisotropic splitting [Eq. (12)] is negligible as compared with the coupling with a magnetic ion. Without the exciton-ion exchange interaction, the ground state of the system "exciton + Mn ion" is (4×6)-fold degenerate. The interaction $\mathcal{H}_{\mathrm{Mn}}$ splits this state into 12 doubly degenerate sublevels half of which, namely, those with the exciton angular-momentum component $m \equiv s+j=\pm 1$, are optically active (or bright). Their energies are given by

$$E_{m,M}^{(S)} = E_0^{(S)} + \delta_s m M, \quad \delta_s = (3I_h^{(s)} - I_e^{(s)})/2, \tag{15}$$

where $E_0^{(S)}$ is the *ss*-shell exciton energy,

$$I_e^{(s)} = \frac{A_e}{\pi a_e^2} e^{-\rho_0^2/a_e^2} \varphi_{e1}^2(z_0), \quad I_h^{(s)} = \frac{A_h}{\pi a_h^2} e^{-\rho_0^2/a_h^2} \varphi_{hh1}^2(z_0),$$

$\rho_0^2=x_0^2+y_0^2$, x_0, y_0, and z_0 are the Cartesian components of $\boldsymbol{r}_0$, and the envelope $\varphi_{e1}(z)$ or $\varphi_{hh1}(z)$ describes the electron or hole confinement along z.

The fine structure of the *pp*-shell exciton excited states is determined by a combined effect of the exciton-Mn and the electron-hole (long-range) exchange interactions. If the QD anisotropy is small so that $|E_a| \ll V_C$, the only bright state $|1\rangle$ defined by Eq. (3) splits into six doubly degenerate sublevels, see Fig. 1(a),

$$E_{m,M}^{(D)} = E_1 + \delta_d m M, \tag{16}$$

where E_1 is the energy of $|1\rangle$ state,

$$\delta_d = \frac{1}{2}(3I_h^{(d)} - I_e^{(d)}), \tag{17}$$

and the coupling constants

$$I_e^{(d)} = \frac{\rho_0^2}{a_e^2} I_e^{(s)}, \quad I_h^{(d)} = \frac{\rho_0^2}{a_h^2} I_h^{(s)} \tag{18}$$

are strongly sensitive to the position of the Mn ion. For example, if the Mn ion is located exactly in the QD center, the splitting of *pp*-shell states vanishes.

In highly anisotropic QDs where $V_C \ll E_a$, the fine structure of the D_{xx} and D_{yy} levels is even more rich. In the general case, an overlap between exciton and Mn ion is different for these two orbitals and one needs to introduce two coupling constants for each type of the carriers, namely,

$$I_e^{(xx)} = \frac{x_0^2}{a_e^2} I_e^{(s)}, \quad I_h^{(xx)} = \frac{x_0^2}{a_h^2} I_h^{(s)}, \tag{19}$$

$$I_e^{(yy)} = \frac{y_0^2}{a_e^2} I_e^{(s)}, \quad I_h^{(yy)} = \frac{y_0^2}{a_h^2} I_h^{(s)}.$$

The eigenenergies are determined by the interplay of the exciton-Mn interaction described by the parameter

$$\delta_{ii} = 3I_h^{(ii)} - I_e^{(ii)} \quad (i=x,y) \tag{20}$$

and the long-range exchange splitting [Eq. (13)]. For a fixed orbital D_{ii}, one should observe six doubly degenerated lines with energies

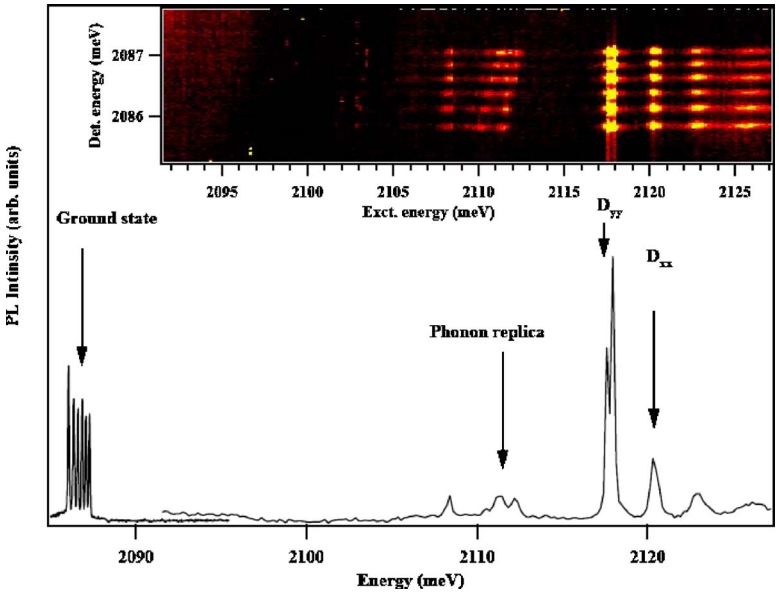

FIG. 2. (Color online) Experimental PL and PLE spectra of Mn-doped quantum dot exciton. The spectral features related to the ground and excited states are marked correspondingly. The inset shows the contour plot of the multichannel PLE.

$$E_{m,M}^{(ii)} = E_{ii} \pm \sqrt{\left(\frac{\delta E_d}{2}\right)^2 + (\delta_{ii} M)^2}, \tag{21}$$

where E_{ii} is the position of the corresponding unperturbed orbital. For $E_d \neq 0$, the levels are nonequidistant and the crossover between anisotropy-dominated regime with two linearly polarized states ($\delta E_d \gg \delta_{ii}$) and the regime of dominant exciton-Mn interaction ($\delta E_d \ll \delta_{ii}$) with six equidistant sublevels takes place.

The fine structure of *sd*-shell states is qualitatively the same. In the isotropic quantum dot, the optically active $s_e d_h$ and $s_h d_e$ shells will be split into six fine sublevels each. The splitting will be determined by the equation similar to Eq. (17). The coupling constants for $s_e d_h$ state will be I_e^s for the electron and $I_h^{sd} = (\rho_0^2/a_h^2 - 1) I_h^s$ for the hole. In the anisotropic quantum dot, each *sd* shell gives rise to two states split due to the confinement anisotropy. The fine structure of each of them is determined, like for *pp* states, by an interplay of long-range exchange interaction and exciton-Mn coupling.

IV. DISCUSSION AND COMPARISON WITH AN EXPERIMENT

We use microspectroscopy to analyze the optical properties of individual Mn-doped self-assembled CdTe/ZnTe QDs. Single Mn atoms are introduced in CdTe/ZnTe QDs

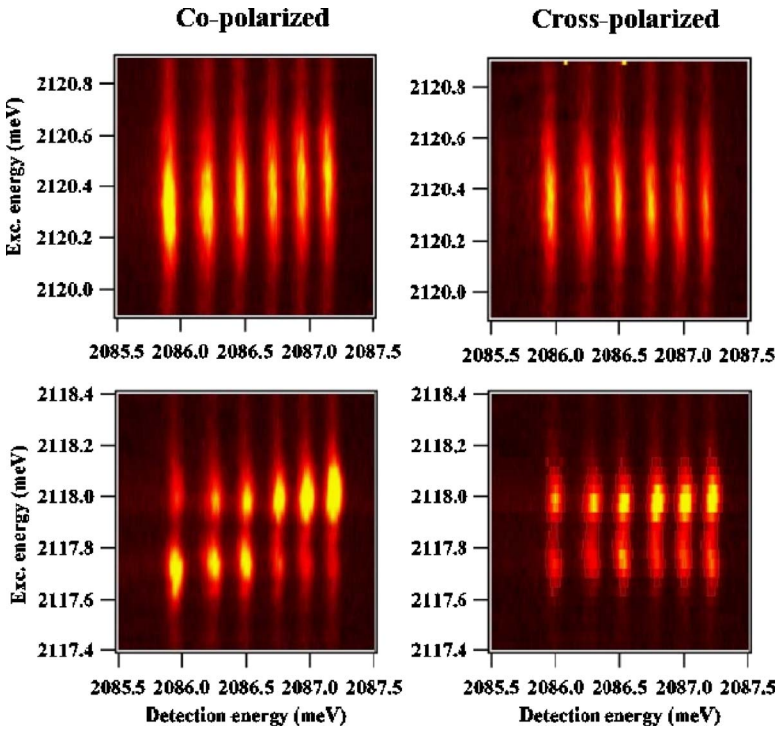

FIG. 3. (Color online) Experimental PLE contour plots for excited states D_{xx} (upper panel) and D_{yy} (lower panels) obtained for copolarized (left panels) and cross-polarized (right panels) circular excitations.

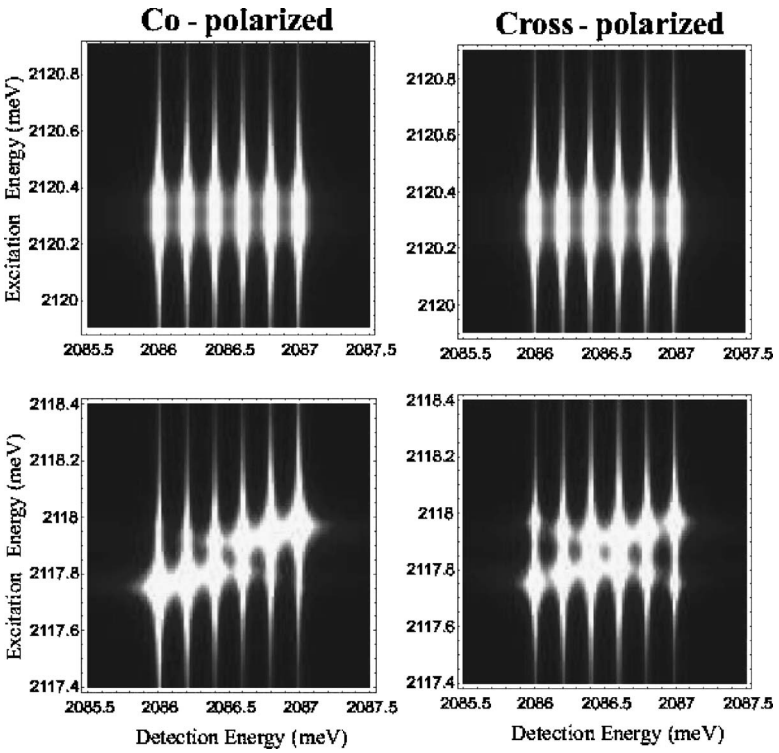

FIG. 4. Calculated PLE spectra in copolarized (left) and cross-polarized (right) configurations. The parameters used are as follows: $E_{yy}=2117.86$ meV, $E_{xx}=2120.30$ meV, $\delta E_d=0.05$ meV, $\delta_{xx}=0.01$ meV, $\delta_{yy}=0.04$ meV, $\delta_s=0.2$ meV, and $E_0^{(S)}=2086.5$ meV. The lines are Lorentzian broadened with the widths $\Gamma_s=0.03$ meV and $\Gamma_{xx}=0.06$ meV, $\Gamma_{yy}=0.03$ meV.

(Refs. 3–5) by adjusting, during the growth process, the density of Mn atoms to be roughly equal to the density of QDs.[15] The PL of individual QDs is excited with a tunable dye laser and collected through aluminum shadow masks with 0.2–1.0 μm apertures. The PL is then dispersed by a 2 m additive double monochromator and detected by a nitrogen-cooled Si charge-coupled device.

The experimental findings for a Mn-doped QD are summarized in Figs. 2–5. This particular QD shows clear linearly polarized excited states. The analysis of the fine structure of other QDs presenting linearly polarized excited states leads qualitatively to the same conclusions. We also note that some QDs demonstrating the excited states in the same energy range present a very weak or nondetectable linear polarization splitting. Figure 2 shows PL and PLE spectra of this QD. The ground-state PL demonstrates six equidistant lines positioned at ~2086 meV. These lines correspond to different projections of Mn spin [see Eq. (15)]. Their approximately equal intensities and regular energy spacing evidence the negligible anisotropic splitting of the ground state. The splitting between these lines suggests the value $\delta_s \approx 0.2$ meV, in good agreement with previous studies.[3]

The first absorption lines in the measured PLE (Fig. 2) lie by ~25 meV above the ground state. This energy range corresponds to the LO-phonon energy between CdTe and ZnTe; thus, this feature can be identified with the phonon replica of the ground state. The nontrivial PLE pattern coming from the replica is a consequence of complicated phonon spectra in such QD system.

Now, we proceed with the discussion of the excited-state fine structure. Two excited states with energies ≈2117.86 and 2120.30 meV are seen in Fig. 2. The sensitivity of the PLE spectra to the linear polarization of excitation, see Fig. 5, evidences the quantum dot anisotropy. Thus, we relate them with the D_{yy}- and D_{xx}-orbital states. The difference in their intensities can be attributed to (i) the shorter lifetime of the highest-energy state and (ii) the Coulomb interaction which, according to Eqs. (3) and (4), intermixes the D_{xx} and D_{yy} states. The latter effect reduces the oscillator strength of the higher state and, as a result, the anisotropic exchange splitting of this state.

A value of the ratio between the energy separation of the excited states D_{xx} and D_{yy} and the distance between ground and excited states allows one to estimate from Eq. (8) the

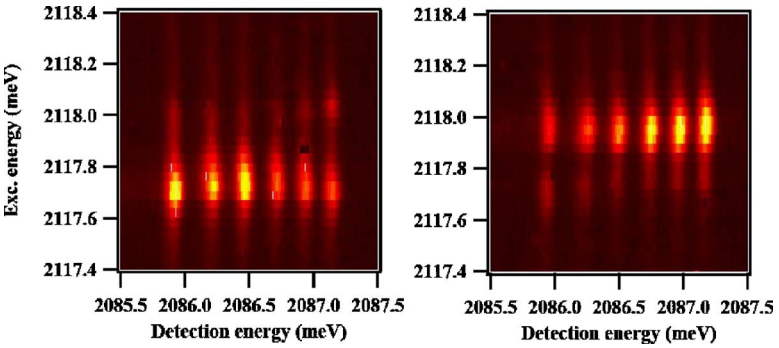

FIG. 5. (Color online) Experimental PLE spectra of D_{yy} states for linearly polarized excitation and unpolarized detection. Left and right panels correspond to two orthogonal linearly polarized excitations.

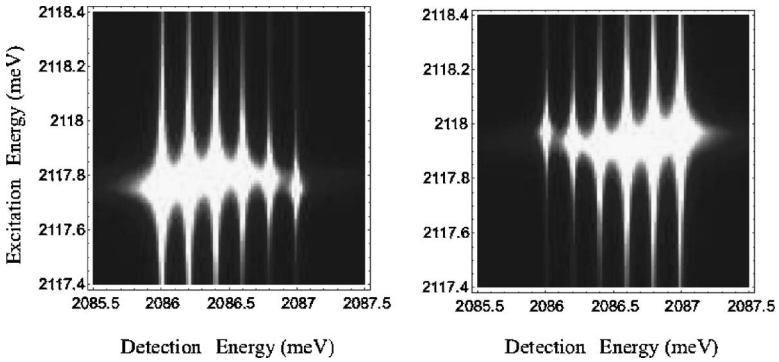

FIG. 6. Calculated PLE spectra for linearly polarized excitation and unpolarized detection. Left and right panels correspond to two orthogonal linear polarizations. The parameters used in the calculation are given in the caption of Fig. 4.

quantum dot anisotropy degree β to be ≈ 0.02, which supports the assumption that the anisotropic splitting of *ss*-shell state is not observed. Figure 2 clearly manifests the splitting of D_{yy} state into a pair of lines. We assume this splitting to come from the QD anisotropy [see Eq. (13)]. The splitting of D_{xx} state is not observed for the reasons suggested above.

The comparison between the experimental data and theoretical predictions in Figs. 3 and 4, respectively, shows that the best possible agreement of the data is obtained for anisotropic splitting $\delta E_d = 0.05$ meV and $\delta_{yy} = 0.04$ meV. The order of magnitude of δE_d is consistent with the quantum dot size $a_e = 45$ Å and $a_h = 90$ Å (i.e., $\zeta = 2$). It agrees with other results for II-VI QDs where the hole confinement is weaker than that of electrons.[16] For these parameters, the predicted energy separation between the ground and excited states is 43 meV, which is somewhat larger than the experimentally observed 33 meV.

Fully quantitative description of the experimental results would require a more complicated theory taking into account all details of the band structure and confinement potential as well as the short-range contribution to the exchange interaction.[17,18]

In order to have a deeper insight into the fine structure of the D_{yy} state, we have performed the PLE measurements for the linearly polarized excitation and unpolarized detection. The experimental results are given in Fig. 5. The theoretical PLE plots calculated for the same parameters as the spectra for circularly polarized excitation are shown in Fig. 6. The reasonable agreement between the theory and experiment is seen. We note that we do not introduce any spin relaxation in the calculations. The similarity in the PL intensity distribution obtained in the theory and in the experiment shows that under resonant excitation, the spin-relaxation time of the exciton-Mn complex is much longer than the lifetime of the exciton: no significant relaxation occurs during the exciton lifetime. As shown in Figs. 3 and 5, this long spin-relaxation time, combined with the fine structure of the excited states, permits to create selectively a given spin configuration of the exciton-Mn complex by tuning the polarization and wavelength of the excitation laser.

Let us note, finally, that the experimentally observed PLE intensity distribution for the higher-energy state D_{xx} is almost uniform, therefore, we conclude that the exciton–Mn-ion coupling is smaller for this state as compared to D_{yy}. We can thus conclude that the Mn ion is located near the y axis. If we completely neglect electron-Mn interaction, using Eq. (20) and the fitted value $\delta_{yy} = 0.04$ meV, we deduce that the Mn-ion is positioned at $y_0 \approx 0.3 a_h$, $x_0 \ll y_0$.

V. CONCLUSION

In conclusion, we have performed a combined experimental and theoretical study of the fine structure of exciton excited states in the QDs containing a single magnetic ion. We have identified two regimes of uniaxial and anisotropic quantum dots where the qualitatively different level arrangements and PLE spectra are predicted. The theoretical results are compared with the experimental data on photoluminescence and photoluminescence excitation for an individual Mn-doped QD. All important experimental observations are reproduced theoretically. The comparison has made it possible to determine the Mn-exciton interaction constants and QD anisotropy degree and to estimate the position of the Mn ion in the quantum dot.

ACKNOWLEDGMENTS

The work was partially supported by RFBR, "Dynasty" foundation-ICFPM, and French ANR contract MOMES.

[1] G. Bacher, A. A. Maksimov, H. Schömig, V. D. Kulakovskii, M. K. Welsch, A. Forchel, P. S. Dorozhkin, A. V. Chernenko, S. Lee, M. Dobrowolska, and J. K. Furdyna, Phys. Rev. Lett. **89**, 127201 (2002).

[2] S. Mackowski, T. Gurung, H. E. Jackson, L. M. Smith, G. Karczewski, and J. Kossut, Appl. Phys. Lett. **87**, 072502 (2005).

[3] L. Besombes, Y. Léger, L. Maingault, D. Ferrand, H. Mariette, and J. Cibert, Phys. Rev. Lett. **93**, 207403 (2004).

[4] L. Besombes, Y. Léger, L. Maingault, D. Ferrand, H. Mariette, and J. Cibert, Phys. Rev. B **71**, 161307(R) (2005).

[5] Y. Léger, L. Besombes, L. Maingault, D. Ferrand, and H. Mariette, Phys. Rev. Lett. **95**, 047403 (2005).

[6] Y. Léger, L. Besombes, L. Maingault, D. Ferrand, and H. Mariette, Phys. Rev. B **72**, 241309(R) (2005).

[7] Y. Léger, L. Besombes, J. Fernández-Rossier, L. Maingault, and H. Mariette, Phys. Rev. Lett. **97**, 107401 (2006).

[8] F. Qu and P. Hawrylak, Phys. Rev. Lett. **96**, 157201 (2006).

[9] A. O. Govorov, Phys. Rev. B **70**, 035321 (2004).

[10] J. Fernández-Rossier, Phys. Rev. B **73**, 045301 (2006).
[11] P. Hawrylak, G. A. Narvaez, M. Bayer, and A. Forchel, Phys. Rev. Lett. **85**, 389 (2000).
[12] Al. L. Efros and M. Rosen, Phys. Rev. B **58**, 7120 (1998).
[13] M. M. Glazov, E. L. Ivchenko, R. v. Baltz, and E. G. Tsitsishvili, arXiv:cond-mat/0501635, Int. J. Nanosci. (to be published).
[14] I. A. Merkulov, D. R. Yakovlev, A. Keller, W. Ossau, J. Geurts, A. Waag, G. Landwehr, G. Karczewski, T. Wojtowicz, and J. Kossut, Phys. Rev. Lett. **83**, 1431 (1999).
[15] L. Maingault, L. Besombes, Y. Leger, and H. Mariette, Appl. Phys. Lett. **89**, 193109 (2006).
[16] B. P. Zhang, W. X. Wang, T. Yasuda, Y. Segawa, K. Edamatsu, and T. Itoh, Appl. Phys. Lett. **71**, 3370 (1997).
[17] I. L. Aleiner and E. L. Ivchenko, Pis'ma Zh. Eksp. Teor. Fiz. **55**, 662 (1992) [JETP Lett. **55**, 692 (1992)].
[18] Alberto Franceschetti and Alex Zunger, Phys. Rev. Lett. **78**, 915 (1997).
[19] We note that for *p*-shell excited states, the Coulomb interaction is the same for P_x and P_y states, and therefore, in the axial approximation, the fine sublevels of *pp* shell are split due to long-range exchange only, see Ref. 13.